Journal of Solid State Electrochemistry (2023) 27:2347–2363
https://doi.org/10.1007/s10008-023-05491-0

ORIGINAL PAPER

Promotion of catalytic activity of Pt@Al-Ti doped ZnO nanostructured anodes for direct methanol fuel cells

Sedigheh Amirinejad[1] · **Jalal Basiri Parsa**[1]

Received: 2 February 2023 / Revised: 22 March 2023 / Accepted: 27 March 2023 / Published online: 24 April 2023

Abstract

Different nanostructured anode electrocatalyst using Pt, Al, Ti, ZnO, and carbon cloth (CC) including Pt@CC, Pt@ZnO-CC, Pt@Al-ZnO-CC, Pt@Ti-ZnO-CC, and Pt@Al-Ti-ZnO-CC are prepared for the purpose of application in direct methanol fuel cells (DMFCs). The effect of carbonaceous material modification and co-doping (Al/Ti) utilization in electrodes is investigated for methanol oxidation reaction (MOR). The results show that the incorporation of Al, Ti, and Pt nanoparticles into ZnO does not damage the hexagonal wurtzite structure. The doping ZnO with Al and Ti nanoparticles improves the dispersion of Pt catalysts and increases the current density by 1.6 times compare with Pt@CC electrode. Maximum electrochemical surface area of 98.6 $m^2\ g^{-1}$, minimum amount of charge transfer resistance of 14 Ω cm^2, and good CO tolerance and stability are found in Pt@Al-Ti-ZnO-CC electrode. This electrode in the active DMFC shows the maximum power and current density of 15.1 mW cm^{-2} and 83.4 mA cm^{-2}, respectively, in the cell voltage of 0.2 V. In the EIS test, charge transfer resistance at the anode and cathode ($R_{ct,a}$ and $R_{ct,c}$) values is decreased by 11.6 and 26.6% by reducing the cell voltage from 0.3 to 0.2 V, respectively.

Keywords Catalytic activity · CO tolerance · Direct methanol fuel cell · Electrocatalyst · Nanostructured electrode · Zinc oxide

Introduction

Direct methanol fuel cells (DMFCs) have attracted considerable scientific interest as one of the next-generation power sources for small and portable applications, due to their high energy density, near zero toxic emission, easy refueling, and fuel security [1]. However, commercialization of DMFCs still confronts major challenges including poor catalytic activity, high-cost materials, and short-term durability [2, 3], which have mostly arisen from the Pt catalyst. These problems may be minimized using the carbonaceous materials and metal oxides as the appropriate Pt supports in methanol oxidation reactions (MORs) [4, 5]. Zinc oxide (ZnO) has received great attention due to its low cost, non-toxicity, environmentally friendly feature and low resistivity [6, 7]. Moreover, ZnO is a transparent conducting oxide (TCO) with outstanding features, which can be considered as a co catalyst. The chemical and thermal stability of metal oxide in the acidic and oxidative media is related to its large band gap (~3.23 eV) [8, 9]. It can promote the catalytic activity and stability of Pt catalysts for MOR, which is the main anodic reaction in the DMFCs. ZnO is able to remove intermediate carbonaceous species (like CO) and prevent CO poisoning during the MOR by the formation of the hydroxyl radicals (OH_{ads}) on the catalyst surface. These hydroxyl groups are produced via the activation of water discharge at low overpotentials [10]. Oxygen vacancy (VO) plays an important role in determining the special properties of ZnO [11, 12]. It was reported that the VO is the electrical charge of Zn^{2+} and the origin of n-type conductivity in ZnO [13]. ZnO has found its place in solar cells [14–16], solid oxide fuel cells (SOFCs) [17–19], semiconductor electronics [20–22], and batteries [23–25]. Huang et al. [26] added ZnO to the catalyst layer as water adsorbent to improve the hydration of electrode surface. Metal doped ZnO films such as Al [27–29], Ga [30, 31], Si [32], Zr [33], and Ti [34, 35] increase the band gap to 3.26 eV and promote the corrosion and oxidation resistant [36, 37]. Doping ZnO with elements of group III, i.e., Al, Ga, and In, as donor atoms can improve the electrical conductivity

✉ Jalal Basiri Parsa
jbparssa@yahoo.com; parssa@basu.ac.ir

[1] Department of Applied Chemistry, Faculty of Chemistry, Bu-Ali Sina University, Hamedan 65178-38695, Iran

and charge transfer process [38]. Co-doping ZnO with Ti and Al as the new trioxide for TCO applications has been reported [38–40].

Doping quantity affects the structure, morphology, and chemical nature of metal oxides. In low concentration, the electrode surface is smooth and uniform [41]. The physical characterizations of doping ZnO with Ti and Al have been reported in the literature [8–11]. However, the practical applications of this nanocomposite could be furthermore investigated. As a result, modified carbonaceous materials and use of Al and Ti nanoparticles in ZnO matrix (ATZO: aluminum titanium-doped zinc oxide) may be considered as the ideal supports for the Pt catalysts in the acidic and oxidative environments of fuel cells.

Based on our knowledge, the electrochemical activity of Pt@Al-Ti-ZnO-CC electrodes for the methanol oxidation in the DMFCs has not been reported yet. So, the aim of this study is to promote the catalytic activity and stability of Pt catalysts and introduce a promising anode for DMFCs. ATZO thin films on carbon cloth (CC) were prepared using the sol–gel and co-precipitation methods. These processes are preferred due to the direct film deposition on the support materials. Besides, they are inexpensive methods in low temperatures with no need of special atmosphere. Pt catalysts were deposited on these supports via airbrushing technique. The prepared electrodes were investigated and compared with Pt@CC electrode. Physical characterizations including scanning electron microscopy (SEM), energy dispersive X-ray analysis (EDX), and X-ray diffraction technique (XRD) were used. The electrochemical surface area (ECSA) and methanol oxidation of the prepared electrodes were determined by cyclic voltammetry (CV) in the acidic media. The stability of the prepared electrodes and the tolerance ability toward CO were investigated via chronoamperometry measurements. The electron transfer resistance of the synthesized electrodes was determined via the electrochemical impedance spectroscopy (EIS). The catalytic activity of the Pt@Al-Ti-ZnO-CC anode was investigated in the active DMFCs.

Experimental

Materials

All chemical materials were purchased from Merck. Pt black with average particle size of below 20 µm was obtained from Sigma-Aldrich. Carbon cloth and Pt/C commercial electrode (0.5 mg cm^{-2}, 60 wt.% Pt on Vulcan-Carbon Cloth) were obtained from Fuel Cell Store. Nafion 117 was bought from Chemours, USA. Deionized (DI) water was used.

Preparation of catalyst support materials

Pt support materials were prepared by the sol–gel and co-precipitation methods according to the scheduled prescription (Table 1). Initially, the CC substrate (1×1 cm^2) was cleaned with acetone, distilled water, and ethanol several times to remove any contaminations [42]. $TiCl_4$ was completely dissolved in the ethanol. The CC was immersed in the solution and was refluxed at 80 °C for 30 min. The CC was dried at 100 °C for 1 h to form Ti layer. Then, $ZnSO_4.7H_2O$ and $Al_2(SO_4)_3.18\ H_2O$ were dissolved in the DI water to form a 0.1 M solution and stirred until a clear solution was observed. The CC was immersed in the solution and NH_4OH (1 M) as precipitator was added dropwise to adjust the pH to 10. The mixture was stirred rapidly at 80 °C for 30 min. The CC was dried at 100 °C for 1 h and finally annealed at 350 °C for 2 h to give ZnO and Al nanoparticles. The proposed reaction mechanism for the synthesis of catalyst supports is shown in Fig. 1.

Preparation of Pt nanoparticles

Pt black was stirred by ultrasound (Sounopuls, HD2200) for 30 min in DI water with loading of 2 mg cm^{-2}. This slurry was coated upon the prepared supports using the spray apparatus (see Fig. 1) and dried for 24 h in the air and then for 2 h in N_2 (99.99%) at 100 °C [43].

Table 1 Composition of the electrodes

Entry	Electrode	ZnO (mol%)	Al (mol%)	Ti (mol%)	Pt (wt.%)
1	Pt@CC	0	0	0	10
2	Pt@ZnO-CC	10	0	0	10
3	Pt@Al-ZnO-CC	10	1	0	10
4	Pt@Ti-ZnO-CC	10	0	0.1	10
5	Pt@Al-Ti-ZnO-CC	10	1	0.1	10

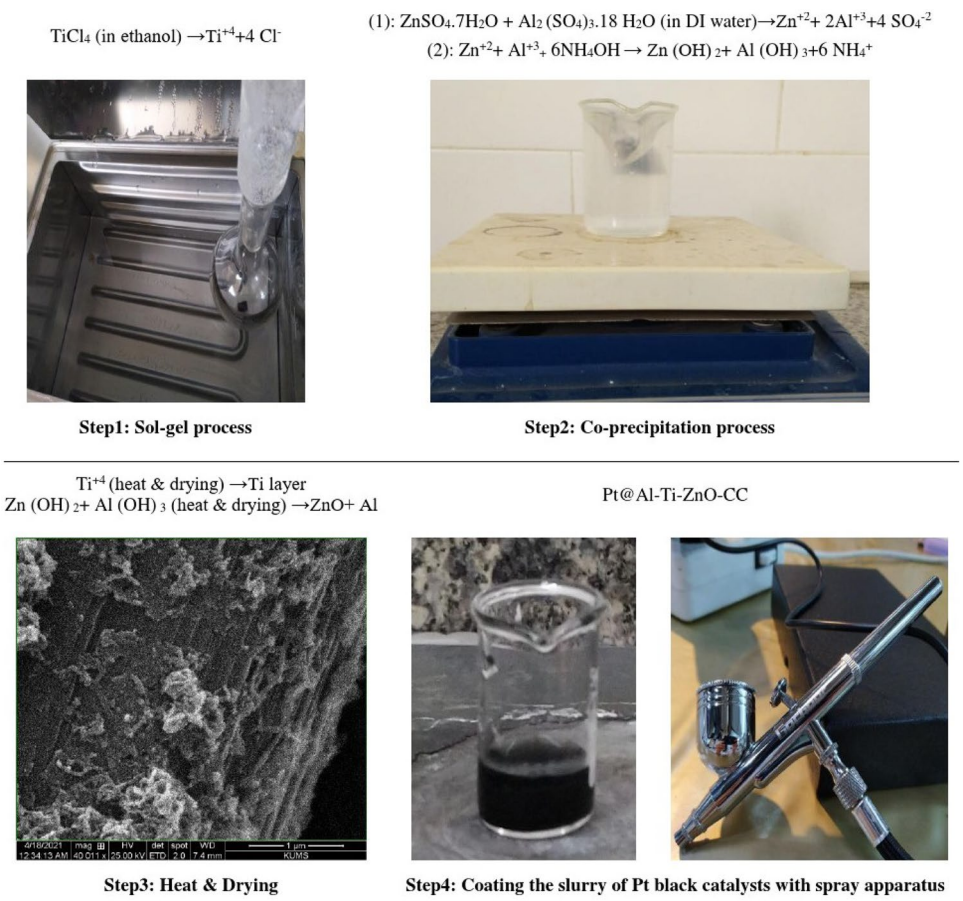

Fig. 1 The proposed reaction mechanism for the synthesis of catalyst supports

Preparation of membrane electrode assembly (MEA)

The effective area of the MEA was 5 cm^2. Pt/C commercial electrode and the prepared Pt@Al-Ti-ZnO-CC electrode were used as the cathode and anode, respectively. Nafion 117 membrane was pretreated for 1 h by 3 wt.% H_2O_2 solution and then rehydrated in the near-boiling 0.5 M H_2SO_4 for about 1 h to reach the protonated form. The membrane was washed by boiling DI water several times and was stored in DI water before use. The MEA was finally fabricated by uniaxially hot-pressing of the electrodes and membrane at temperature of 130 °C and pressure of 120 atm for 3 min [43]. The MEA was placed in a gold-plated fuel cell hardware (AHNS Co.) and then connected to the fuel cell test station (Scribner-Associates, USA).

Physical analysis

SEM, SERON technology, AIS2100 was used to observe the surface morphology of the prepared electrodes. To recognize the elemental composition, the EDX technique with an accelerating voltage of 15 kV was applied. The crystal structures of the prepared electrodes were examined by X-ray diffractometry (XRD-Rigakuultima iv, Japan).

Electrochemical measurement

Electrochemical tests were performed in Autolab potentiostat instrument (PGSTAT302N). Three-electrode cell was used including the prepared electrodes, Pt rod (Metrohm, $d = 2$ mm) and the standard calomel electrode (SCE; Metrohm 6.07.29.100) as working, the counter and the reference electrodes, respectively. Before testing, the degasification of solution was performed by high purity nitrogen bubbling. The ECSA was determined by hydrogen under potential deposition (H_{upd}) region measured by the CV recorded between -0.4 and + 1.3 V vs SCE in 0.5 M H_2SO_4 at a scan rate of 50 mV s^{-1}. Electrooxidation of methanol was examined by the CV between 0 and 1.3 V at a scan rate of 50 mV s^{-1} in 0.5 M H_2SO_4 containing 1 M methanol. The chronoamperometry was measured by polarization of electrodes at the peak potential of CV for 1200 s in 0.5 M H_2SO_4 containing 1 M methanol. EIS was carried out in 0.5 M H_2SO_4 containing 1 M methanol. The Nyquist plots were obtained at a near peak potential of MOR at a frequency range of 100 kHz to 100 mHz with 10 mV as the amplitude of the sine wave. All experiments were performed at room temperature (~25 °C).

MEA activation

Initially, the MEA was activated by off-line and on-line preconditioning procedures [44], respectively. In the off-line method, electrodes were exposed to the water steam for 1 h. In the on-line method, the MEA was activated by a constant voltage at 0.6 V for 6 h. By these activations, the electrodes were hydrated, the contaminants were eliminated, and the active sites of the catalyst layer were readied for reaction with methanol. The performance of the MEA was investigated in the active DMFC. Methanol solution in the concentrations from 1 to 5 M and the flowrate of 1 mL min^{-1} at 60 °C (near its boiling point) were used. Pure oxygen was fed to the cathode by the flowrate of 100 mL min^{-1}. Current/voltage curves were obtained by scanning the cell voltage in the range of open-circuit voltage up to 100 mV with a scan rate of 20 mV s^{-1} at 40, 50, and 60 °C. Meanwhile, the EIS investigation was carried out in the ranges of 100 kHz -10 mHz and the optimum operations (3 M methanol, 60 °C) at 0.2 and 0.3 V. The AC signal amplitude was 5% of the DC current.

Results and discussion

Characterization of synthesized electrodes

The surface of Al-Ti doped ZnO on the CC electrodes is shown in Fig. 2. The nonporous and interconnected structure is seen. The average particles size of the nanoparticles was between 30 and 60 nm. Al and Ti doped ZnO nanoparticles improved the dispersion of Pt nanoparticles and increased the electrochemical surface area. In other words, Al-Ti nanoparticles caused more homogeneous dispersion of Pt nanoparticles, which created more active catalytic sites for MORs.

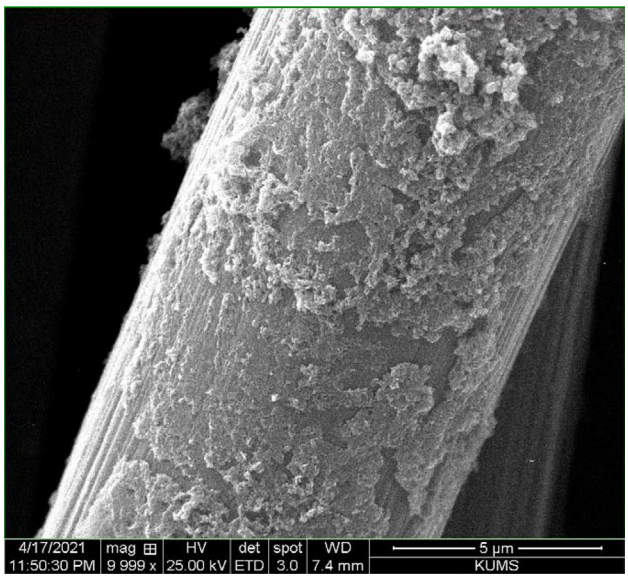

Fig. 2 SEM image of Al and Ti doped ZnO on carbon cloth electrode

The shape of Pt nanoparticle is spherical granule (Fig. 3). The average particle size of Pt on CC, ZnO-CC, Al-ZnO-CC, Ti-ZnO-CC, and Al-Ti-ZnO-CC was about 70, 100, 80, 90, and 95 nm, respectively. As shown in Fig. 3, the use of Al and Ti nanoparticles in the electrode composition decreased the average particles size of Pt.

EDX analysis of prepared electrodes is shown in Fig. 4. The peaks attributed to Zn, Al, Ti, C, and Pt are presented in the EDX spectrum. The results confirmed that Pt and metal oxides were successfully deposited on CC.

The XRD of prepared electrodes is displayed in Fig. 5. As seen, the diffraction peaks at 26 and 43.5° corresponded to the (002) and (100) planes of graphitic carbon (JCPDS card no. 08–0415), indicating the amorphous nature of CC [45]. The diffraction peeks around 32.06, 34.71, 36.51, 47.79, and 56.84° can be indexed to the (100), (002), (101), (102), and (110) planes of the hexagonal wurtzite structure of ZnO (JCPDS no. 36–1451) [46]. Doping Al and Ti nanoparticles with ZnO kept the crystal structure of ZnO as reported in the literature [40]. The relatively sharp XRD patterns demonstrated the crystallinity of prepared Pt@Al-Ti-ZnO nanoparticles. Al, Ti, and Pt have been incorporated into the crystal structure of ZnO [47]. There were no characteristic peaks of impurities in the pattern. It is concluded that the preparation method used in this study is very reliable to synthesize ATZO thin films.

Electrochemical characterization

ECSA

Figure 6a indicates the cyclic voltammograms of prepared electrodes in N_2-saturated 0.5 M H_2SO_4 solution. The electrochemically active surface area of the electrodes was also estimated from the integrated charge in the hydrogen adsorption and deposition region from the electrode surface of CVs. The potential ranges from -0.25 to 0.15 V represent the hydrogen adsorption/deposition region. The Coulombic charge (Q_H) of monolayer of H_2 adsorbed on Pt between -0.25 and + 0.15 V vs. SCE in CV was then obtained. The ECSA of electrodes was calculated using Eq. (1):

$$ECSA = \frac{Q_H}{210 \times L_{Pt}} \quad (1)$$

In this equation, Q_H is the Coulombic charge for hydrogen adsorption on Pt sites, L_{Pt} is the loading of Pt in the working electrode, and the number of 210 is the electrical charge required to oxidize a monolayer of hydrogen on Pt surface [48].

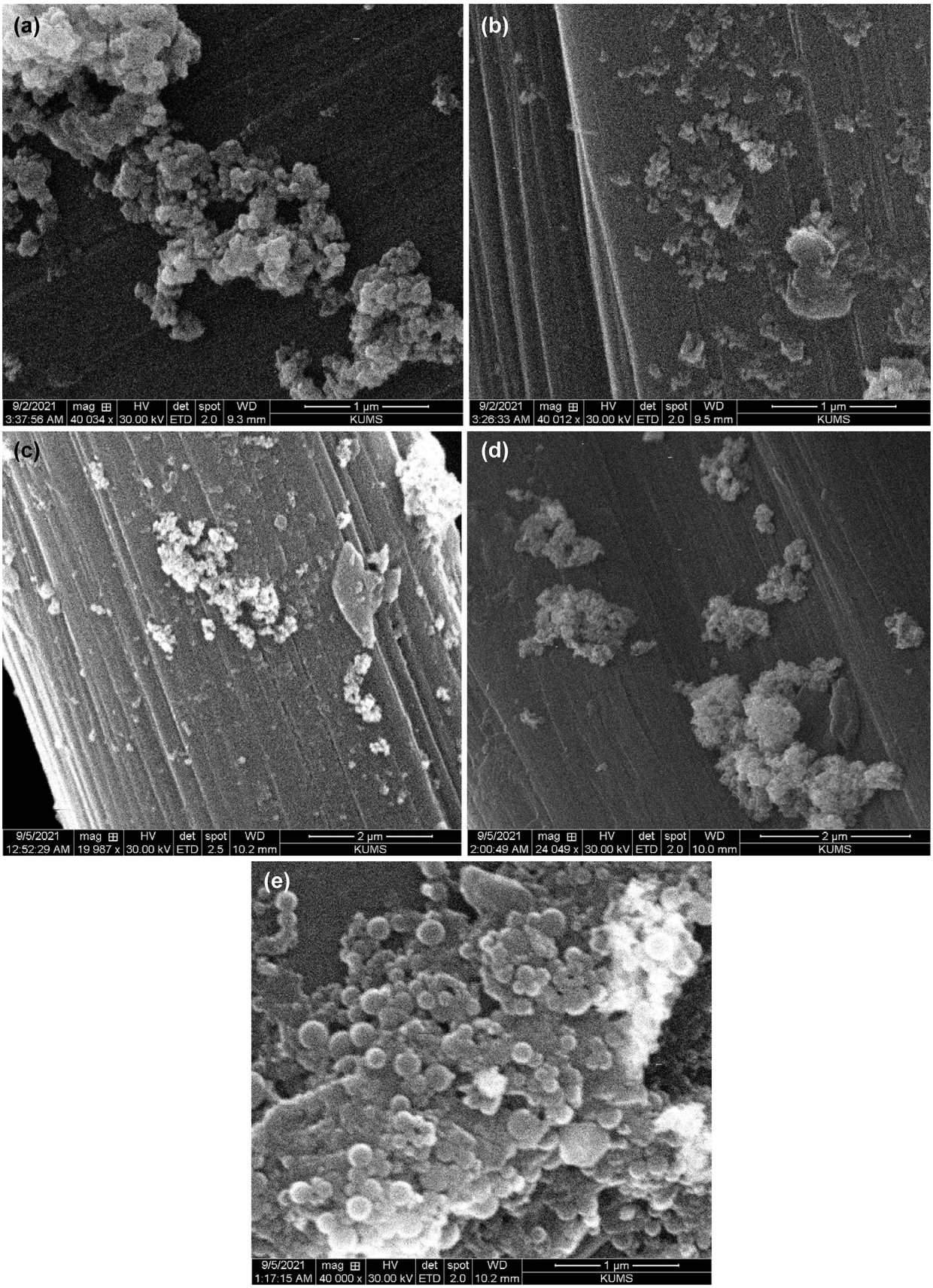

Fig. 3 SEM images of the (**a**) Pt@CC, (**b**) Pt@ZnO-CC, (**c**) Pt@Al-ZnO-CC, (**d**) Pt@Ti- ZnO-CC, and (**e**) Pt@Al-Ti-ZnO-CC electrodes

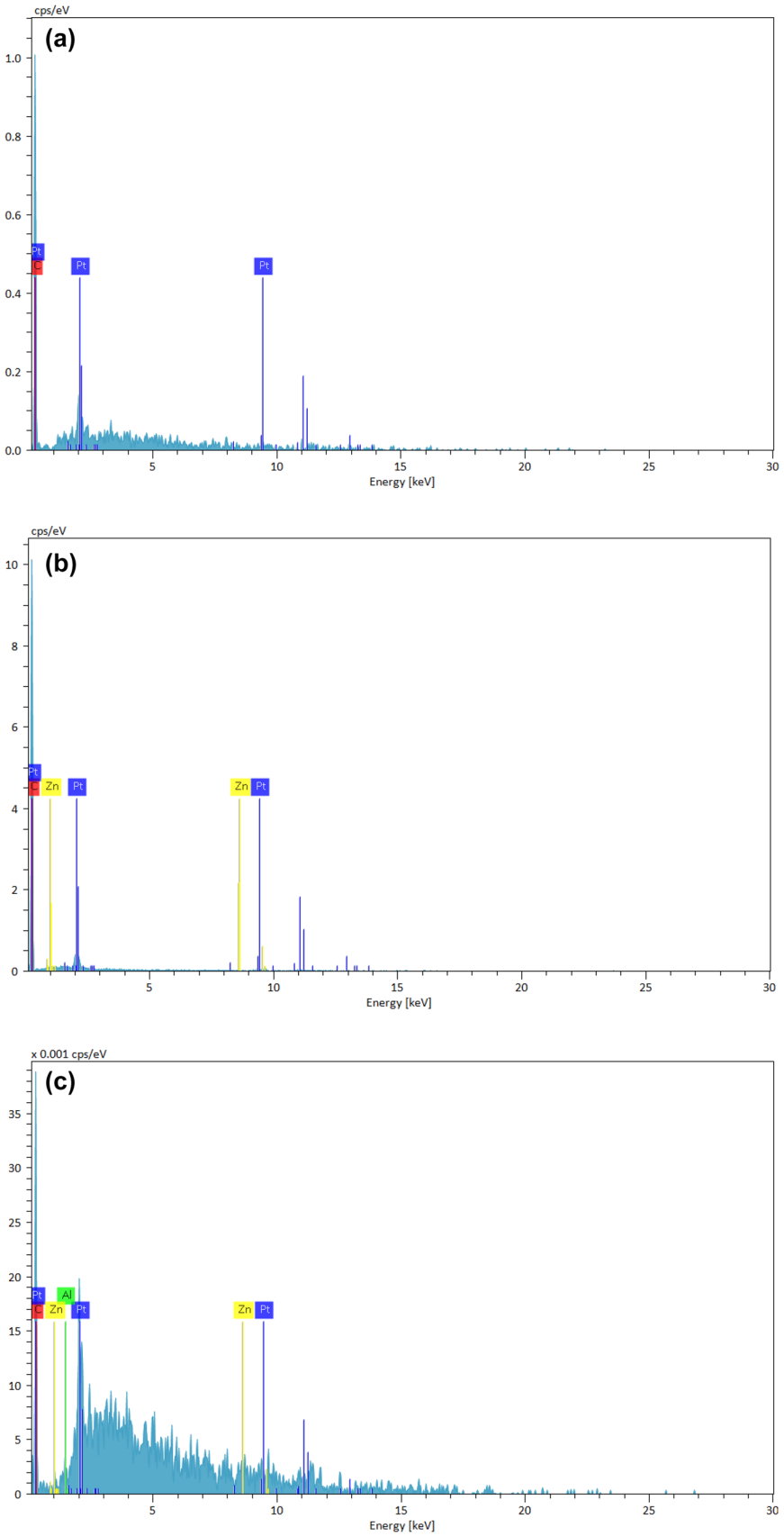

Fig. 4 EDX analysis of (**a**) Pt@CC, (**b**) Pt@ZnO-CC, (**c**) Pt@Al-ZnO-CC, (**d**) Pt@Ti- ZnO-CC, and (**e**) Pt@Al-Ti-ZnO-CC electrodes

Fig. 4 (continued)

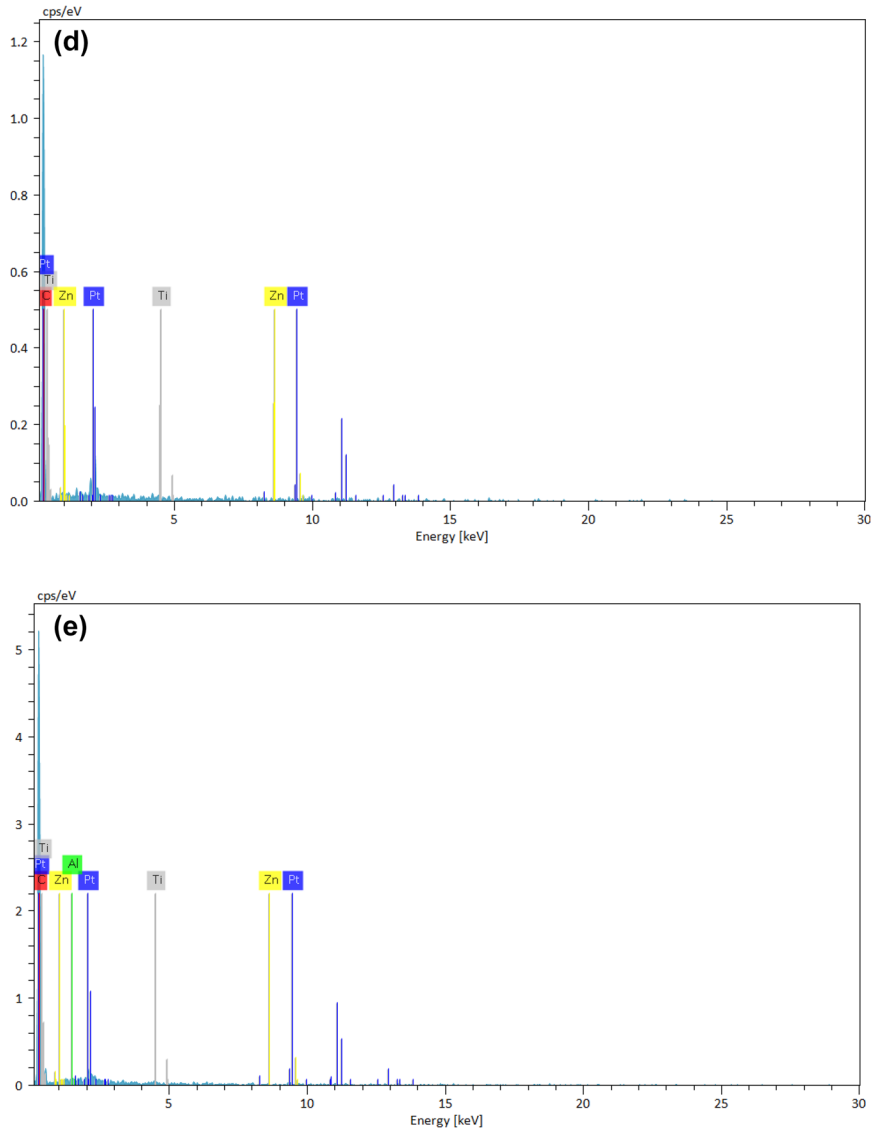

The ECSA values of Pt@CC, Pt@ZnO-CC, Pt@Al-ZnO-CC, Pt@Ti-ZnO-CC, and Pt@Al-Ti-ZnO-CC were 21.1, 66.7, 79.4, 92.3, and 98.6 $m^2\ g^{-1}$, respectively (Fig. 6b). These results showed that the ECSA of electrodes increased by doping of ZnO with Al and Ti. The support modification and the use of ATZO improved the Pt catalyst dispersion and enhanced the electrochemical surface area which affected the stability and lowering the cost. The highest ECSA value was measured for Pt@Al-Ti-ZnO-CC electrode, which indicated the most accessible active sites toward the MOR. As a result, the high ECSA of Pt may be due to high electrical conductivity and surface area of ATZO, suggesting a relation between ECSA and electronic conductivity of the support materials.

Alcohol electrooxidation

Figure 7 shows the CV measurements of the prepared electrodes for methanol oxidation. The electrochemical parameters obtained from the CV have been tabulated in Table 2. In this table, E_p, I_f, I_r, and I_f/I_r are the peak potential, the current density of forwarding peak, the current density of reverse peak, and the ratio of forwarding peak current to reverse peak current, respectively [48]. The CV values displayed well-defined peaks in the anodic scan, which confirmed the good Pt catalyst activation for MOR [49]. The current density of Pt@Al-Ti-ZnO-CC electrode at the peak potential of 0.82 V was 107 mA cm^{-2}. The identical Pt loading on the prepared electrodes increased the current density

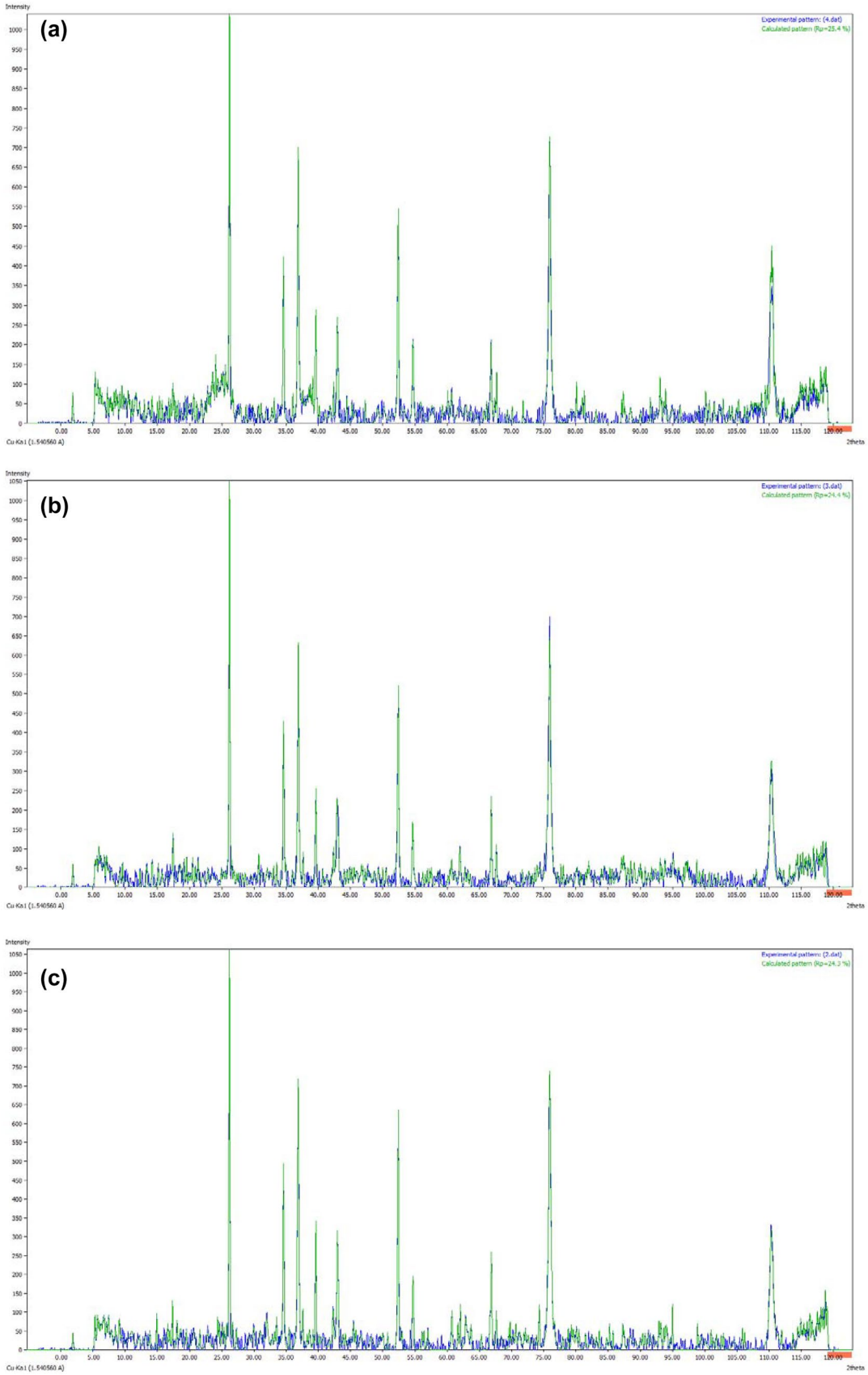

Fig. 5 X-ray patterns of (**a**) Pt@ZnO-CC, (**b**) Pt@Al-ZnO-CC, (**c**) Pt@Ti- ZnO-CC, and (**d**) Pt@Al-Ti-ZnO-CC electrodes

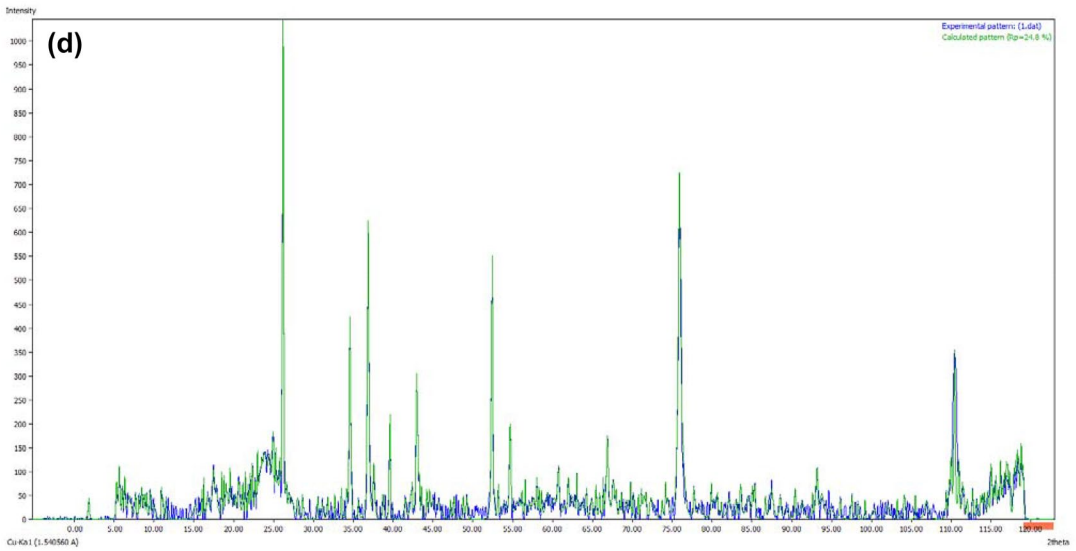

Fig. 5 (continued)

by 1.6 times compared to Pt@CC electrode, which may be attributed to the higher electrochemical surface area of Pt@Al-Ti-ZnO-CC electrode compared to Pt@CC electrode. The increase in the surface area may be attributed to the coverage of CC surface with Al and Ti doped ZnO nanoparticles (see SEM images).

I_f/I_r values for Pt@CC, Pt@ZnO-CC, Pt@Al-ZnO-CC, Pt@Ti-ZnO-CC, and Pt@Al-Ti-ZnO-CC were 1.7, 2, 2.1, 2.4 m and 3.4, respectively. Since the large I_f/I_r ratio indicated high CO tolerance ability and stability of electrodes [48], doping ZnO with Al and Ti increased I_f/I_r values for the prepared electrodes and improved the Pt catalyst activity toward CO poisoning [50].

The peak potential, E_p on Pt@Al-Ti-ZnO-CC electrode was located at a lower potential and a reduction of about 0.05 V in the overpotential reaction was found when compared to Pt@CC electrode. As the lower amount of E_p means more oxidizing ability [51], doping Al and Ti with ZnO promoted the catalytic activity of the Pt catalysts.

Generally, the high electrical conductivity, the high electrochemical surface area, and the high CO tolerance are three essential properties that should be considered for the supporting materials in MORs [51, 52]. Among the prepared electrodes, Pt@Al-Ti-ZnO-CC exhibited the highest electrical conductivity, electrochemical surface area, and CO tolerance, as described, below.

Pt nanoparticles on the relatively stable nanocomposite and interaction between the Pt and the ATZO nanocomposite and the high levels of electrical conductivity due to the efficient existence of the dopant atoms are two main reasons for this phenomena. As the results showed, doping ZnO with Al and Ti led to the appropriate formation of active catalytic sites for MORs.

Chronoamperometry test

Chronoamperometry measurement of the prepared electrodes for the methanol oxidation is indicated in Fig. 8. Methanol can be oxidized continuously on the catalyst surface at the peak potential [48]. As seen, the current density decreased rapidly at the first and then reached a steady-state due to the formation of Pt oxide or the adsorbed intermediate species such as CO_{ads} on the Pt catalyst surface [53]. When the electrocatalyst has good physical–chemical stability and poisoning-resistance, this decreasing slope is mild and gradual. The initial current densities of Pt@CC, Pt@ZnO-CC, Pt@Al-ZnO-CC, Pt@Ti-ZnO-CC, and Pt@Al-Ti-ZnO-CC were 67, 78, 84, 92, and 107 mA cm^{-2}, respectively. Pt@Al-Ti-ZnO-CC electrode had the most ECSA value and the most available catalytic active sites for methanol oxidation and showed the highest initial current density. After 1200 s, the current densities of Pt@CC, Pt@ZnO-CC, Pt@Al-ZnO-CC, Pt@Ti-ZnO-CC, and Pt@Al-Ti-ZnO-CC dropped to 8.1, 16.4, 17.4, 32, and 40.8 mA cm^{-2}, respectively. The final current density for Pt@Al-Ti-ZnO-CC electrode was fivefold greater compared to the Pt@CC electrode. It may be attributed to the larger ECSA value and higher oxidation ability toward CO-like intermediate. Intermediate species could be strongly adsorbed on Pt@CC electrode during MOR and blocked the catalytic reaction active sites [51]. Synergistic effect of advanced oxidation process of ZnO in removal of CO_{ads} from the catalyst surface is illustrated in Fig. 9. In ZnO semiconductor, the electron (e^-) can be conducted from its valence band (VB) to the conduction band (CB) at low overpotentials. The outcome of this phenomenon is formation of holes in VB (h^+) that will act as oxidizing sites as described in Fig. 9. In h^+ of ZnO surface, H_2O acts as electron donor and generates $OH°$. Hydroxyl radicals can

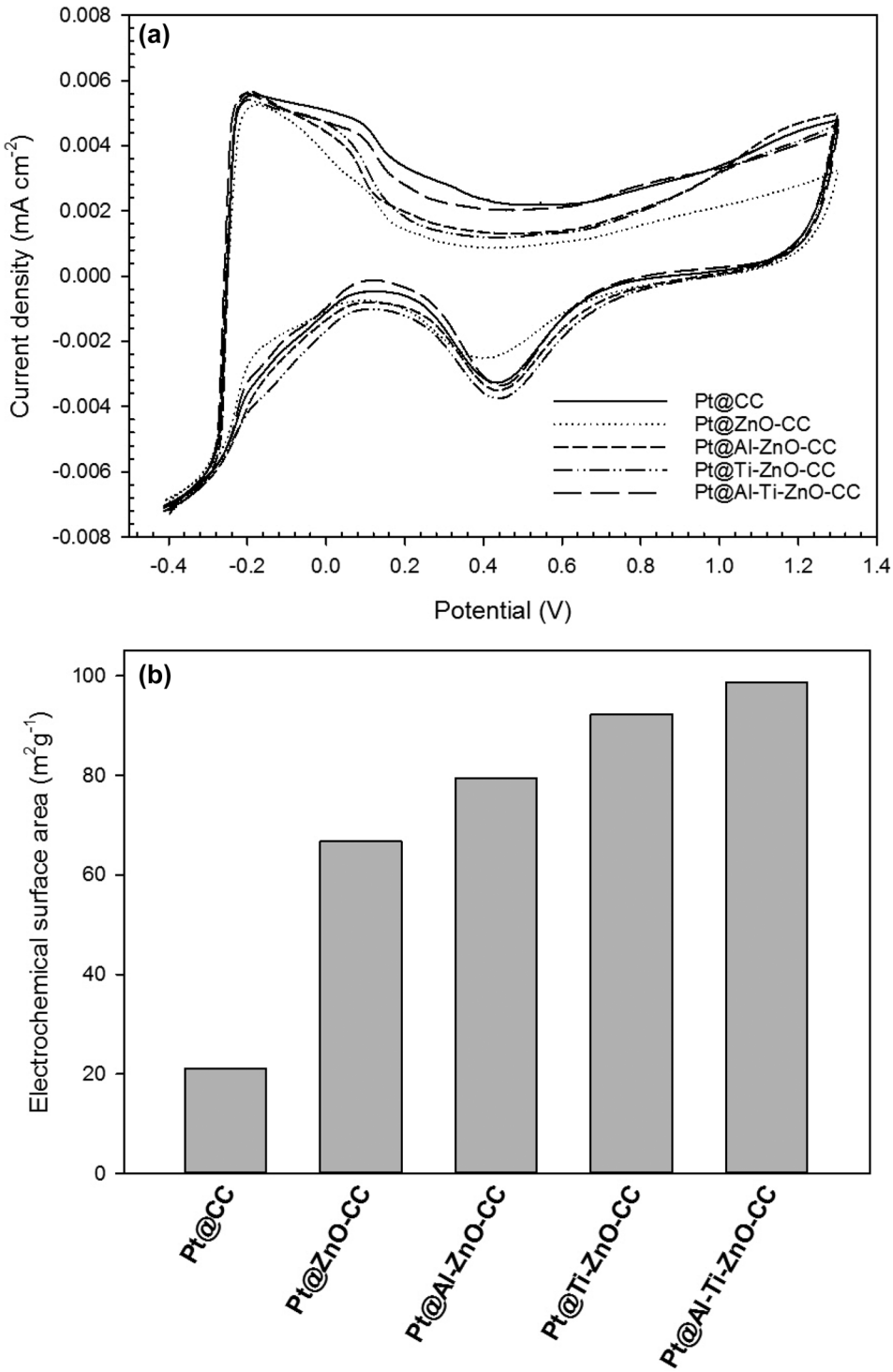

Fig. 6 (**a**) Cyclic voltammograms of the electrocatalysts in H_2SO_4 solution (0.5 M) and (**b**) ECSA data for the electrocatalysts

oxidize CO_{ads} and prevent Pt from poisoning. Poisoning rate (δ) and stability of prepared catalysts are calculated from the chronoamperograms using Eq. (2) [54]:

$$\delta = {}^{100}/_{i_0} \times (di/dt)_{t\rangle 200s} \text{ (\% per second)} \quad (2)$$

where, i_0 is the current obtained by the extrapolating the linear current decay and $(di/dt)_{t\rangle 200s}$ is the slope of linear current at $t > 200\,s$. The long-term poisoning values for Pt@CC, Pt@ZnO-CC, Pt@Al-ZnO-CC, Pt@Ti-ZnO-CC, and Pt@Al-Ti-ZnO-CC catalysts were calculated 0.16, 0.1, 0.07,

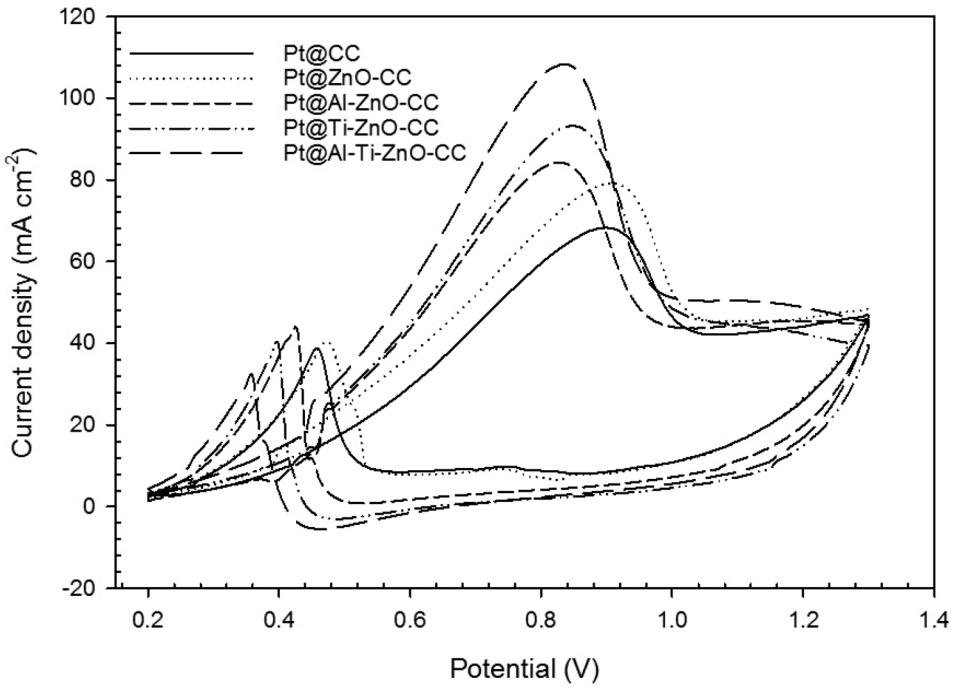

Fig. 7 Cyclic voltammograms of the electrocatalysts in H_2SO_4 solution (0.5 M) + CH_3OH solution (1 M)

0.05, and 0.03% per second in the methanol, respectively. As results show, Al-Ti co-doped ZnO support material enhanced CO tolerance of Pt catalyst, which may be attributed to the high electrical conductivity and interaction between the Pt catalyst and ATZO support material. Similarly, the electronic effect between Pt and ATZO led to the proper adsorption of *OH*° on Pt sites and removal of the carbonaceous intermediate species during the MOR. Furthermore, the strong metal oxide interaction could hinder the aggregation of Pt nanoparticles. It is important to note that the prepared electrodes keep their alcohol oxidation activity even after 1200 s despite a rapid activity loss at the initial stage.

EIS

Figure 10 displays the EIS Nyquist plots and the equivalent circuit for prepared electrodes. The equivalent circuit was obtained by fitting the impedance data using Autolab NOVA software. In this circuit, Z_w, R_s, R_{ct}, and C_{dl} are the Warburg impedance, the solution resistance, the charge transfer resistance, and the double layer capacitance, respectively. The faster oxidation reaction rate of alcohol led to lower R_{ct} value and higher electrocatalytic activity [51]. Based on the obtained results, the R_{ct} values of Pt@CC, Pt@ZnO-CC, Pt@Al-ZnO-CC, Pt@Ti-ZnO-CC, and Pt@Al-Ti-ZnO-CC were 38.5, 26.8, 24.9, 18.1, and 14 Ω cm^2 in methanol, respectively. The minimum amount of R_{ct} was obtained for Pt@Al-Ti-ZnO-CC electrode. These results confirmed the other findings. Al-Ti doped ZnO can produce hydroxyl radicals and oxidize the intermediate carbonaceous species on the Pt catalyst surface. Likewise, ATZO increased the electrical conductivity that improved the catalytic activity of Pt.

Table 2 Electrochemical characterization of methanol oxidation

Entry	Electrode	E_p (V)	I_f (mA cm^{-2})	I_r (mA cm^{-2})	I_f/I_r
1	Pt@CC	0.87	67	38.5	1.7
2	Pt@ZnO-CC	0.87	78	39	2
3	Pt@Al-ZnO-CC	0.82	84	40.6	2.1
4	Pt@Ti-ZnO-CC	0.82	92	38.5	2.4
5	Pt@Al-Ti-ZnO-CC	0.82	107	31.7	3.4

Active DMFC

Figure 11 shows the polarization and power density curves of the MEA by changing the methanol concentration. It is clear that the cell activity increased after increasing methanol concentration from 1 to 3 M. The lower methanol concentration, i.e., 1 M, was associated with a severe rate of polarization during the high-current operation, due to the difficulty in absorbing sufficient amount of methanol. In contrast, the cell performance declined at concentrations of 4 and 5 M. The use of higher methanol concentrations, e.g., 4 and 5 M, inevitably induced the methanol crossover (MCO) from the anode to the cathode [55]. The highest power densities and potential values at all current densities were observed in 3 M methanol concentration. In this concentration, the current densities of 28.6, 45.4, 66.6, 74.8,

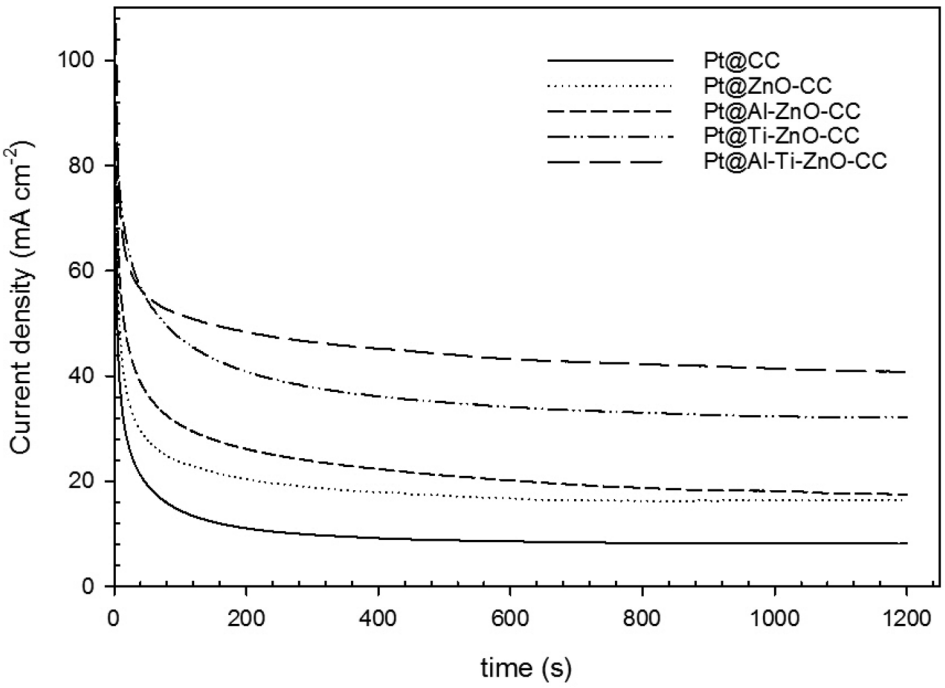

Fig. 8 Chronoamperometric curves of the electrocatalysts for the methanol oxidation in H_2SO_4 solution (0.5 M) + CH_3OH solution (1 M)

96.5, and 108.8 mA cm^{-2} were achieved at 0.3, 0.26, 0.22, 0.2, 0.14, and 0.1 V, respectively.

The peak power density of the MEA was 15.1 mW cm^{-2} and a current density of 83.4 mA cm^{-2} at a cell voltage of 0.2 V was obtained in 3 M methanol concentration.

The polarization and power density curves of the MEA by changing the operating temperature are shown in Fig. 12. As expected, the cell performance improved with increasing the temperature due to the increment in the rates of MOR and ORR (oxygen reduction reaction) at the anode and cathode, respectively [56]. However, an increase in the rate of MCO and a decrease in the membrane quality function are inevitable [57]. As previously reported [58, 59], at higher temperatures than 80 °C, membrane drying increased MCO values and then catalyst deterioration occurred. The current densities of 14.2, 21, 31.4, 44.5, 54, and 66.1 mA cm^{-2} were obtained at 0.3, 0.26, 0.22, 0.2, 0.14, and 0.1 V, respectively, at 40 °C. Similarly, the current densities of 22.9, 32.1, 44.5, 51.4, 65, and 79 mA cm^{-2} were taken at 0.3, 0.26, 0.22, 0.2, 0.14, and 0.1 V, respectively, at 50 °C. The peak power densities were 8.4, 10.4, and 15.1 mW cm^{-2} at 40, 50, and 60 °C, respectively.

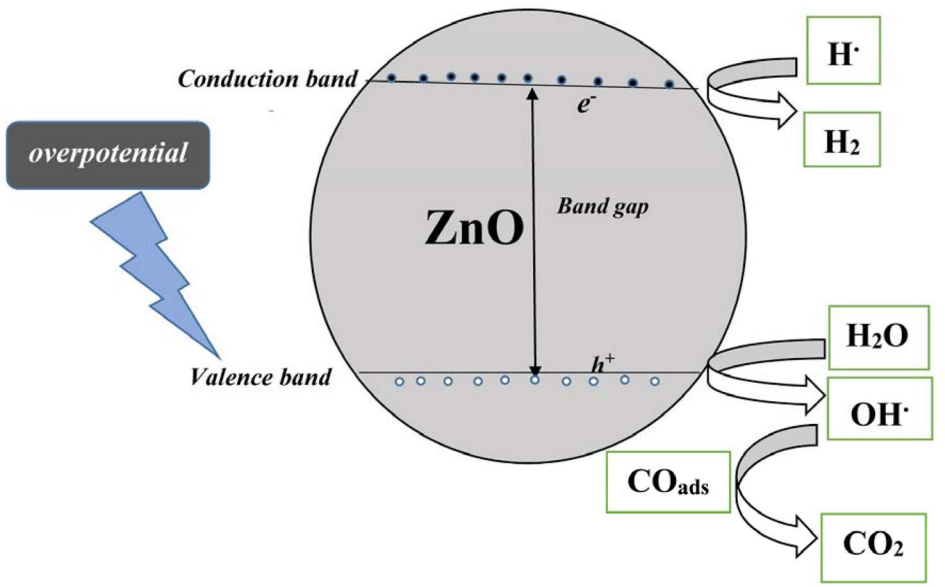

Fig. 9 Synergistic effect of ZnO advanced oxidation process

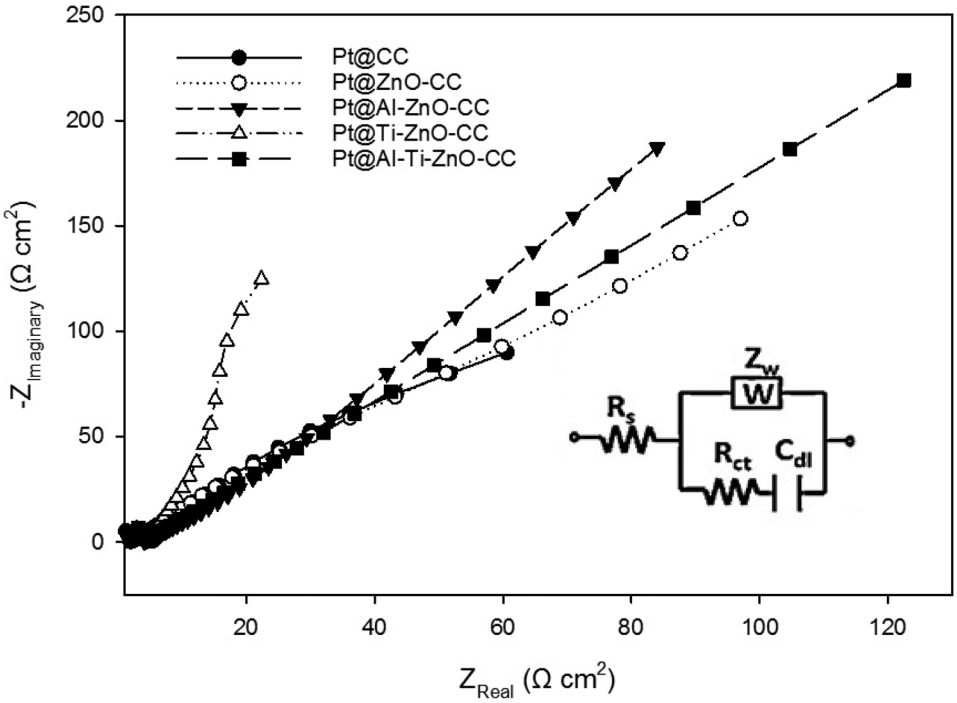

Fig. 10 EIS Nyquist plots (dots) and equivalent circuit for the electrocatalysts in H_2SO_4 solution (0.5 M) + CH_3OH solution (1 M)

The EIS Nyquist plots at 0.3 and 0.2 V for the MEA in 3 M methanol at 60 °C were measured and showed in Fig. 13. The equivalent circuit was determined by fitting the impedance data using Zview software (Fig. 13). Two arcs in the high and low frequency areas of the impedance spectrum were observed due to the low rate of MOR and ORR in DMFCs, respectively [60, 61]. The equivalent circuit parameters are tabulated in Table 3. $R_{ct,a}$ is the charge transfer resistance at the anode, $R_{ct,c}$ is the charge transfer resistance at the cathode, CPE-a and CPE-c are the double layer capacitances at the anode and cathode, respectively. R_{ohm} is the bulk resistance and is attributed to the proton exchange membrane. In this case, R_{ohm} values are close to each other in 0.2 and 0.3 V potentials due to the same MEA with the similar hydration level. By reducing the cell voltage from 0.3 to 0.2 V, $R_{ct,a}$ and $R_{ct,c}$ values decreased by 11.6 and 26.6%, respectively. As a result, the reduction of the cell voltage provided the reactions activation energy and the resistance to the charge transfer at the electrode surface decreased.

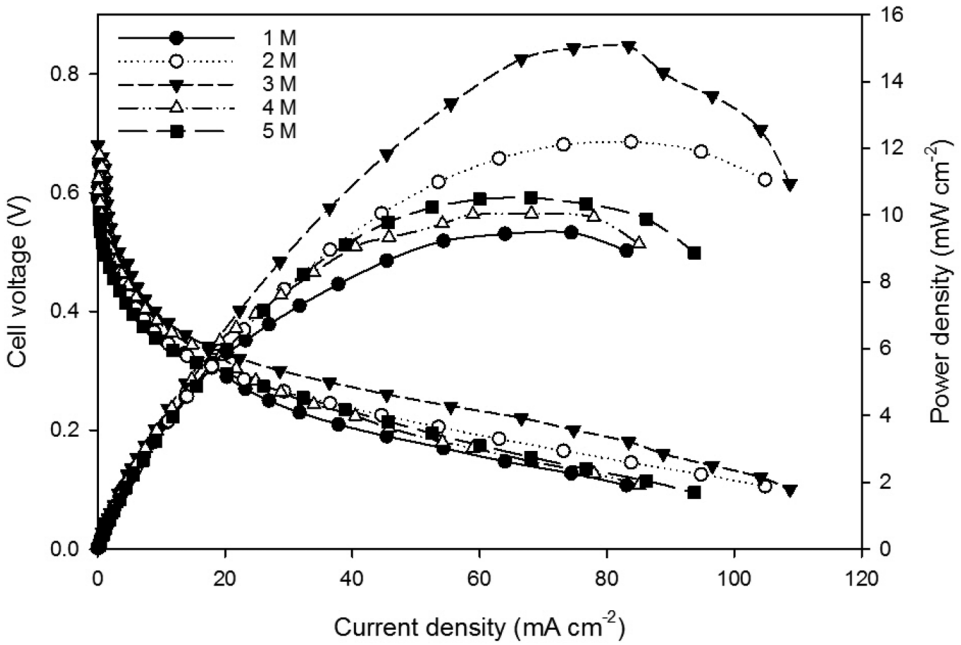

Fig. 11 Polarization and power density for the MEA at different methanol concentrations at 60 °C

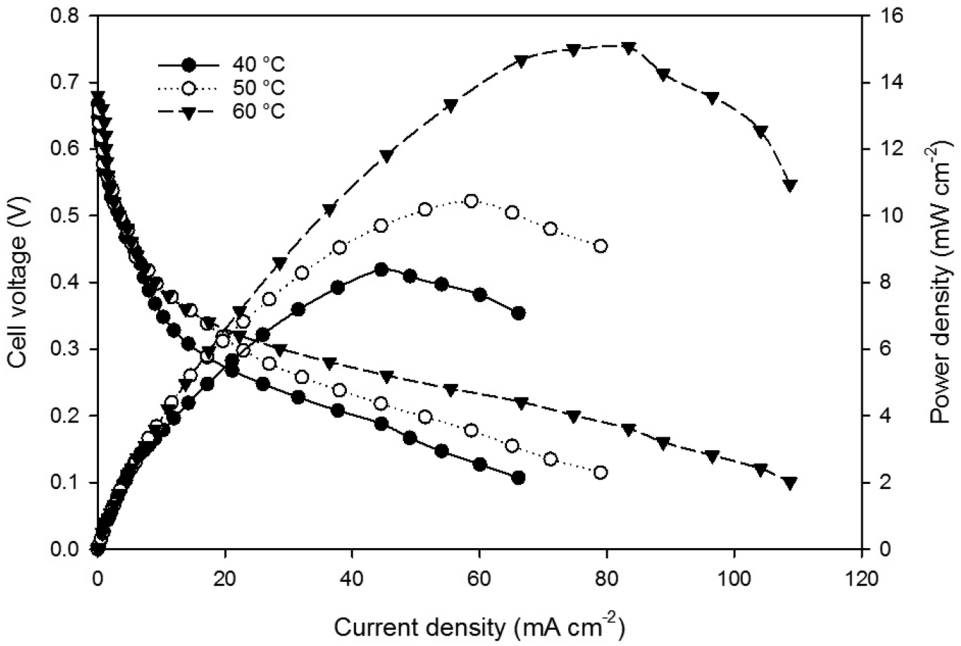

Fig. 12 Polarization and power density for the MEA at different temperatures by consuming methanol solution (3 M)

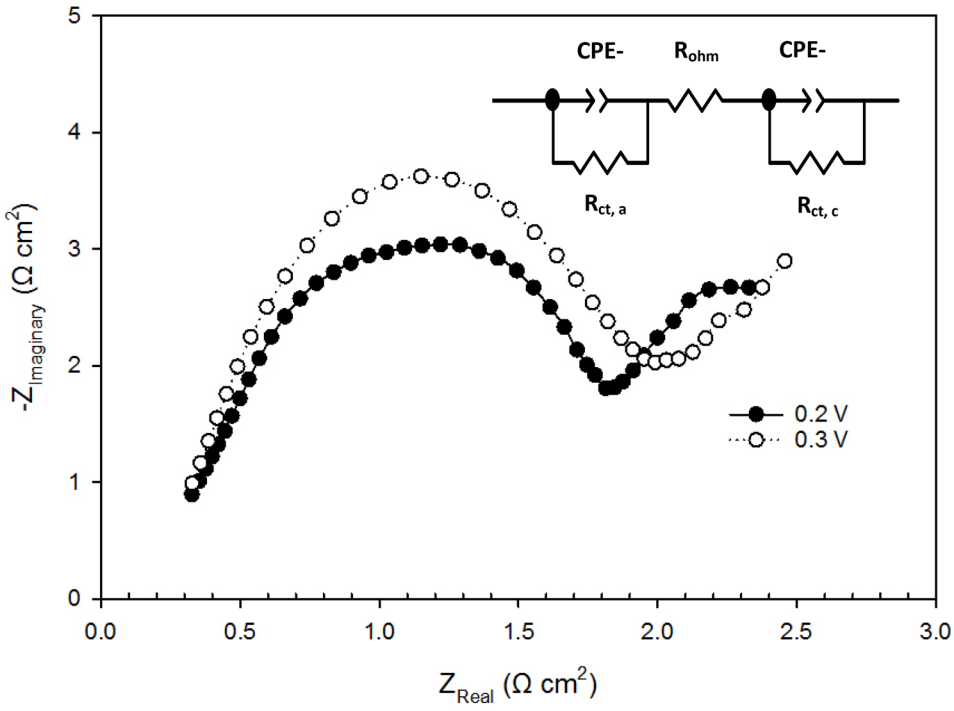

Fig. 13 EIS Nyquist plots (dots) and equivalent circuit for the MEA at 0.2 V and 0.3 V

Table 3 The obtained fitting EIS data of prepared MEA in the fuel cell

Entry	Cell voltage (V)	R_{ohm} (Ω cm^2)	$R_{ct,a}$ (Ω cm^2)	$R_{ct,c}$ (Ω cm^2)	CPE-a (mF cm^{-2})	CPE-c (mF cm^{-2})
1	0.2	0.32	1.67	1.71	1.031	331
2	0.3	0.33	1.89	2.33	0.978	582

Conclusion

The catalyst Pt@Al-Ti-ZnO-CC was synthesized by the sol–gel and co-precipitation methods. Physical analysis and electrochemical measurements of the prepared electrocatalyst were investigated in half and whole cell of MOR by the electrochemical techniques.

SEM images confirmed the nonporous and interconnected structure for the synthesized ATZO. The average particle size of Pt decreased by the use of Al and Ti nanoparticles in the electrode composition. XRD patterns revealed the purity and crystallinity of the synthesized Pt@Al-Ti-ZnO nanoparticles on CC.

Electrochemical characterization results showed the higher catalytic activity of Pt@Al-Ti-ZnO-CC in terms of stability, electrical conductivity, electrochemical surface area, and I_f compared to Pt@CC for MOR in the acidic media.

Finally, the highest peak power density for the MEA was obtained in 3 M methanol and 60 °C. Pt@Al-Ti-ZnO-CC as the anode revealed excellent activity for DMFCs.

Abbreviations

ATZO: Aluminum titanium-doped zinc oxide; CB: Conduction band; CC: Carbon cloth; CO: Carbon monoxide; CO_{ads}: Adsorbed carbon monoxide; CV: Cyclic voltammetry; DI: Deionized; DMFC: Direct methanol fuel cell; ECSA: Electro chemical surface area; EDX: Energy dispersive X-ray analysis; EIS: Electrochemical impedance spectroscopy; H_{upd}: Hydrogen under potential deposition; MCO: Methanol crossover; MEA: Membrane electrode assembly; MOR: Methanol oxidation reaction; ORR: Oxygen reduction reaction; SEM: Scanning electron microscopy; TCO: Transparent conducting oxide; VB: Valence band; VO: Oxygen vacancy; XRD: X-ray diffraction

List of symbols

δ: Poisoning rate/% per second; CPE-a: Double layer capacitance at the anode/mF cm^{-2}; CPE-c: Double layer capacitance at the cathode/mF cm^{-2}; C_{dl}: Double layer capacitance/μF cm^{-2}; E_p: Peak potential/V; i_0: Current obtained by the extrapolating the linear current decay/mA cm^{-2}; I_f: Current density of forwarding peak/mA cm^{-2}; I_r: Current density of reverse peak/mA cm^{-2}; L_{Pt} : Pt loading/g_{Pt} m^{-2}; Q_H: Coulombic charge for hydrogen adsorption on the Pt sites/μC cm^{-2}; R_{ct}: Charge transfer resistance/Ω cm^2; $R_{ct,a}$: Charge transfer resistance at the anode/Ω cm^2; $R_{ct,c}$: Charge transfer resistance at the cathode/Ω cm^2; R_{ohm}: Bulk resistance/Ω cm^2; R_s: Solution resistance/Ω cm^2; Z_w: Warburg impedance/Ω cm^2; $(di/dt)_{t\rangle 200s}$: Linear current slope at $t > 200\,s$/mA cm^{-2} s^{-1}

References

1. Ho VTT, Pham HQ, Anh THT, Nguyen AV, Quoc KAN, Vo HTH, Nguyen TT (2019) Highly stable Pt/ITO catalyst as a promising electrocatalyst for direct methanol fuel cells. C R Chimie 22:838–843
2. Nguyen AKQ, Huynh TT, Ho VTT (2016) Highly stable Pt/ITO catalyst as a promising electrocatalyst for direct methanol fuel cells. Mol Cryst Liq Cryst 635:32–39
3. Yavari Z, Noroozifar M, Khorasani-M M (2016) The improvement of methanol oxidation using nano-electrocatalysts. J Exp Nanosci 11:798–815
4. Berghian-GC RT, Biris AR, Dan M, Voica C, Watanabe F (2020) Platinum nanoparticles coated by graphene layers: a low-metal loading catalyst for methanol oxidation in alkaline media. J Energy Chem 40:81–88
5. Li J, Zhao L, Li X, Hao S, Wang Z (2020) Fabrication of C@MoTi1-O_2-δnanocrystalline with functionalized interface as efficient and robust PtRu catalyst support for methanol electrooxidation. J Energy Chem 40:7–14
6. Jafarova VN, Orudzhev GS (2021) Structural and electronic properties of ZnO: a first-principles density-functional theory study within LDA(GGA) and LDA(GGA) + U methods. Solid State Commun 325:114166
7. Patil SA, Jagdale PB, Singh A, Singh RV, Khan Z, Samal AK, Saxena M (2023) 2D zinc oxide–synthesis, methodologies, reaction mechanism, and applications. Small. https://doi.org/10.1002/smll.202206063
8. Davoodi A, Tajally M, Mirzaee O, Eshaghi A (2016) Fabrication and characterization of optical and electrical properties of Al-Ti Co-doped ZnO nano-structured thin film. J Alloy Compd 657:296–301
9. Coguplugil KZ, Akin M, Bayat R, Bekmezci M, Karimi-Maleh H, Javadi A, Sen F (2022) Synthesis and characterization of Pt/ZnO@SWCNT/Fe_3O_4 as a powerful catalyst for anodic part of direct methanol fuel cell reaction. Int J Hydrogen Energy. https://doi.org/10.1016/j.ijhydene.2022.10.238
10. Wang H, Wang X, Zheng J, Peng F, Yu H (2015) Enhanced activity and durability of nanosized Pt–SnO_2/IrO_2/CNTs catalyst for methanol electrooxidation. J Nanosci Nanotechnol 15:3662–3669
11. Tu Y, Chen S, Li X, Gorbaciova J, Gillin WP, Krause S, Briscoe J (2018) Control of oxygen vacancies in ZnO nanorods by annealing and their influence on ZnO/PEDOT:PSS diode behavior. J Mater Chem C 6:1815–1821
12. Nowicka E, n Althahban SM, Luo Y, Kriegel R, Shaw G, Morgan DJ, He Q, Watanabe M, Armbrüster M, Kiely CJ, Hutchings GJ (2018) Highly selective PdZn/ZnO catalysts for the methanol steam reforming reaction. Catal Sci Technol 8:5848–5857
13. Liu L, Mei Z, Tang A, Azarov A, Kuznetsov A, Xue Q-K, Du X (2016) Oxygen vacancies: the origin of n-type conductivity in ZnO. APS Phys 93:235305
14. Hussain B, Ebong A, Ferguson I (2015) Zinc oxide as an active n-layer and antireflection coating for silicon based heterojunction solar cell. Sol Energy Mater Sol Cells 139:95–100
15. Pietruszka R, Schifano R, Krajewski TA, Witkowski BS, Kopalko K, Wachnicki L, Zielony E, Gwozdz K, Bieganski P, Placzek-Popko E, Godlewski M (2016) Improved efficiency of n-ZnO/p-Si based photovoltaic cells by band offset engineering. Sol Energy Mater Sol Cells 147:164–170
16. Mahdi MA, Yousefi SR, Jasim LS, Salavati-Niasari M (2022) Green synthesis of $DyBa_2Fe_3O_{7.988}$/$DyFeO_3$ nanocomposites using almond extract with dual eco-friendly applications: photocatalytic and antibacterial activities. Int J Hydrogen Energy 47:14319–14330

17. Qiao Z, Xia C, Cai Y, Afzal M, Wang H, Qiao J, Zhu B (2018) Electrochemical and electrical properties of doped CeO_2-ZnO composite for low-temperature solid oxide fuel cell applications. J Power Sources 392:33–40
18. Xia C, Mi Y, Wang B, Lin B, Chen G, Zhu B (2019) Shaping triple-conducting semiconductor BaCo0.4Fe0.4Zr0.1Y0.1O3-δ into an electrolyte for low-temperature solid oxide fuel cells. Nat Commun 10:1707
19. Yousefi SR, Ghanbari M, Amiri O, Marzhoseyni Z, Mehdizadeh P, Hajizadeh-Oghaz M, Salavati-Niasari M (2021) Dy_2BaCuO_5/$Ba_4DyCu_3O_{9.09}$ S-scheme heterojunctionnanocomposite with enhanced photocatalytic and antibacterial activities. J Am Ceram Soc 104:2952–2965
20. Yousefi SR, Alshamsi HA, Amiri O, Salavati-Niasari M (2021) Synthesis, characterization and application of Co/Co_3O_4 nanocomposites as an effective photocatalyst for discoloration of organic dye contaminants in wastewater and antibacterial properties. J Mol Liq 337:116405
21. Yousaf SM, Mushtaq MN, Rauf S, Xia C, Zhu B (2019) The semiconductor SrFe0.2Ti0.8O3-δ-ZnO heterostructure electrolyte fuel cells. Int J Hydrogen Energy 44:30319–30327
22. Mukhamedshina D, Mit K, Chuchvaga N, Tokmoldin N (2017) Fabrication and study of sol-gel ZnO films for use in Si-based heterojunction photovoltaic devices. MoEM 3:158–161
23. Thauer E, Zakharova GS, Andreikov EI, Adam V, Wegener SA, Nölke J-H, Singer L, Ottmann A, Asyuda A, Zharnikov M, Kiselkov DM, Zhu Q, Puzyrev IS, Podval'naya NV, Klingeler R (2021) Novel synthesis and electrochemical investigations of ZnO/C composites for lithium-ion batteries. J Mater Sci 56:13227–13242
24. Yousefi SR, Amiri O, Salavati-Niasari M (2019) Control sonochemical parameter to prepare pure Zn0.35Fe2.65O4 nanostructures and study their photocatalytic activity. Ultrason Sonochem 58:104619
25. Yousefi SR, Masjedi-Arani M, Sadat Morassaei M, Salavati-Niasari M, Moayedi H (2019) Hydrothermal synthesis of $DyMn_2O_5$/$Ba_3Mn_2O_8$ nanocomposite as a potential hydrogen storage material. Int J Hydrogen Energy 44:24005–24016
26. Huang R-H, Chiu T-W, Lin T-J, Sun C-H, Chao W-K, Hsueh K-L, Shieu F-S, Tsai D-C (2013) Improvement of proton exchange membrane fuel cells performance by coating hygroscopic zinc oxide on the anodic catalyst layer. J Power Sources 227:229–236
27. Yousefi SR, Sobhani A, Salavati-Niasari M (2017) A new nanocompositesuperionic system ($CdHgI_4$/HgI_2): synthesis, characterization and experimental investigation. Adv Powder Technol 28:1258–1262
28. Kim YS, Tai WP (2007) Electrical and optical properties of Al-doped ZnO thin films by sol-gel process. Appl Surf Sci 253:4911
29. Hao XT, Tan LW, OngKS ZhuF (2006) High-performance low-temperature transparent conducting aluminum-doped ZnO thin films and applications. J Cryst Growth 287:44
30. Saito K, Hiratsuka Y, Omata A, Makino H, Kishimoto S, Yamamoto T, Horiuchi N, Hirayama H (2007) Atomic layer deposition and characterization of Ga-doped ZnO thin films. Superlattices Microstruct 42:172
31. Mehdizadeh P, Jamdar M, Mahdi MA, Abdulsahib WK, Jasim LS, Yousefi SR, Salavati-Niasari M (2023) Rapid microwave fabrication of new nanocomposites based on Tb-Co-O nanostructures and their application as photocatalysts under UV/Visible light for removal of organic pollutants in water. Arab J Chem 16:104579
32. Das D, Karmakar L (2020) Optimization of Si doping in ZnO thin films and fabrication of n-ZnO:Si/p-Si heterojunction solar cells. J Alloy Compd 824:153902
33. Bian H, Ma S, Yang G, Zhu H, Xu X, Yan S, Gao J, Zhang Z (2016) The optical and electrical properties of ZnO: Zr films. J Alloy Compd 48:20–26
34. Ye Z-Y, Lu H-L, Geng Y, Gu Y-Z, Xie Z-Y, Zhang Y, Sun Q-Q, Ding S-J, Zhang DW (2013) Structural, electrical, and optical properties of Ti-doped ZnO films fabricated by atomic layer deposition. Nanoscale Res Lett 8:108
35. Hosseini J, Bodaghi A (2011) Preparation of palladium nanoparticles–titanium electrodes as a new anode for direct methanol fuel cells. J Solid State Electrochem 15:795–800
36. Wang J, Xu J, Chen Z, Wang X (2023) Multi-dimensional Pt–Mo/Co@NC nanocomposites with low platinum contents for methanol oxidation. J Solid State Electrochem 27:327–336
37. Jiang M, Hu Y, Zhang W, Wang L, Yang S, Liang J, Zhang Z, Zhang X, Jin Z (2021) Regulating the alloying degree and electronic structure of Pt–Au nanoparticles for high-efficiency direct C_{2+} alcohol fuel cells. Chem Mater 33:3767–3778
38. Bocchese F, Cornil D, Haye E, Cornil J, Lucas S (2022) Three-zone model for Ti, Al co-doped ZnO films deposited by magnetron sputtering. Surf Interfaces 28:101595
39. Lin J, Wu JN, Tseng CA, Peng KC (2013) Effect of direct current power to Ti-target on the composition, structure and characterization of the Ti (0–2.36 at. %), Al codoped ZnO sputtering thin films, Jpn J Appl Phys 52:01 AC06
40. Lin J, Huang M, Wang T, Wu J, Tseng Y, Peng KC (2015) Structure and characterization of the sputtered ZnO, Al-doped ZnO, Ti-doped ZnO and Ti, Al-co-doped ZnO thin film. Mater Express 5:153–158
41. Shimaa MA, Hamedh AAL (2017) Nano-structured sol-gel coatings as protective films against zinc corrosion in 0.5 M HCl solution. J Saudi Chem Soc 21:473–480
42. Narayanasamy S, Jayaprakash J (2021) Carbon cloth/nickel cobaltite ($NiCo_2O_4$)/polyaniline (PANI) composite electrodes: preparation, characterization, and application in microbial fuel cells. Fuel 301:121016
43. Amirinejad M, Rowshanzamir S, Eikani MH (2006) Effects of operating parameters on performance of a proton exchange membrane fuel cell. J Power Sources 161:872–875
44. Taghiabadi MM, Zhiani M, Silva V (2019) Effect of MEA activation method on the long-term performance of PEM fuel cell. Appl Energy 242:602–611
45. Gao Z, Yang W, Wang J, Song N, Li X (2015) Flexible all-solid-state hierarchical $NiCo_2O_4$/porous grapheme paper asymmetric supercapacitors with an exceptional combination of electrochemical properties. Nano Energy 13:306–317
46. Singh A, Vishwakarma HL (2015) Study of structural, morphological, optical and electroluminescent properties of undoped ZnO nanorods grown by a simple chemical precipitation. Mater Sci Pol 33:751–759
47. Radicic R, Maletic D, Blažeka D, Car J, Krstulovi N (2022) Synthesis of silver, gold, and platinum doped zinc oxide nanoparticles by pulsed laser ablation in water. J Nanomater 12:3484
48. Merati Z, BasiriParsa J (2018) Enhancement of the catalytic activity of Pt nanoparticles toward methanol electro-oxidation using doped-SnO_2 supporting materials. Appl Surf Sci 435:535–542
49. Dinesh B, Saraswathi R (2016) Enhanced performance of Pt and Pt-Ru supported PEDOT-RGO nanocomposite towards methanol oxidation. Int J Hydrogen Energy 41:13448–13458
50. Peng K, Bhuvanendran N, Ravichandran S, Zhang W, Ma Q, Xu Q, Xing L, Khotseng L, Su H (2020) Bimetallic Pt_3Mn nanowire network structures with enhanced electrocatalytic performance for methanol oxidation. Int J Hydrogen Energy 45:30455–30462
51. Li M, Zhao S, Han G, Yang B (2009) Electrospinning-derived carbon fibrous mats improving the performance of commercial Pt/C for methanol oxidation. J Power Sources 191:351–356
52. Merati Z, BasiriParsa J (2018) Electrochemically synthesized polypyrrole/MWCNTs-Al_2O_3 ternary nanocomposites supported

Pt nanoparticles toward methanol oxidation. Int J Hydrogen Energy 43:20993–21005
53. Yasmeen N, Rahman G, Mehmood M, Bilal S (2016) Electrooxidation of methanol at PANI/POAP bilayered structure modified platinum and graphite electrodes. Electrochim Acta 188:367–377
54. Gharibi H, Amani M, Pahlavanzadeh H, Kazemeini M (2013) Investigation of carbon monoxide tolerance of platinum nanoparticles in the presence of optimum ratio of doped polyaniline with para toluene sulfonic acid and their utilization in a real passive methanol fuel cell. Electrochim Acta 97:216–225
55. Baronla R, Goel J, Kaswan J, Shukla A, Singhal SK, Singh SP (2018) PtCo/rGO nano-anode catalyst: enhanced power density with reduced methanol crossover in direct methanol fuel cell. Mater Renew Sustain Energy 7:27
56. Yuan W, Wang A, Yan Z, Tan Z, Tang Y, Xia H (2016) Visualization of two-phase flow and temperature characteristics of an active liquid-feed direct methanol fuel cell with diverse flow fields. Appl Energy 179:85–98
57. Li H, Zhao H, Tao B, Xu G, Gu S, Wang G, Chang H (2022) Pt-based oxygen reduction reaction catalysts in proton exchange membrane fuel cells: controllable preparation and structural design of catalytic layer. J Nanomater 12:4173
58. Zhang Z, Yang T, Li Y, Li J, Yang Q, Wang L, Jiang L, Su B (2022) Effects of expanded hemodialysis with medium cut-off membranes on maintenance hemodialysis patients: a review. Membranes 12:253
59. Devrim Y, Erkan S, Bac N, Eroglu I (2012) Improvement of PEMFC performance with Nafion/inorganic nanocomposite membrane electrode assembly prepared by ultrasonic coating technique. Int J Hydrogen Energy 37:16748–16758
60. Ercelik M, Ozden A, Seker E, Colpan CO (2017) Characterization and performance evaluation of Pt-Ru/C-TiO2 anode electrocatalyst for DMFC applications. Int J Hydrogen Energy 42:21518–21529
61. Braz BA, OliveiraVB PAMFR (2020) Experimental evaluation of the effect of the anode diffusion layer properties on the performance of a passive direct methanol fuel cell. Energies 13:5198